Line Roughness in Lamellae-Forming Block Copolymer Films

Ricardo Ruiz,*[,†] Lei Wan,[†] Rene Lopez,[‡] and Thomas R. Albrecht[†]

[†]HGST, a Western Digital Company, San Jose, California 95135, United States

[‡]Department of Physics and Astronomy, University of North Carolina at Chapel Hill, Chapel Hill, North Carolina 27599, United States

ABSTRACT: We study the line roughness in poly(styrene-*b*-methyl methacrylate) symmetric block copolymer thin films and propose a phenomenological model to fit and describe the observed line edge, width, and placement roughness. Owing to the layering structure of symmetric block copolymers, we build from the model used to describe the thermal fluctuations in bilayer membranes and add a term for the bulk composition fluctuations in a phase segregated system. We use the peristaltic and undulatory modes of bilayer membranes to describe the width and placement roughness, respectively. We also include the correlations between adjacent domains to capture the cross-talk between alternating domains. We find that the model reproduces most of the main features observed in the power spectral density of our block copolymer films, providing a baseline to understand the physical properties that influence line roughness in a system relevant to nanolithography.

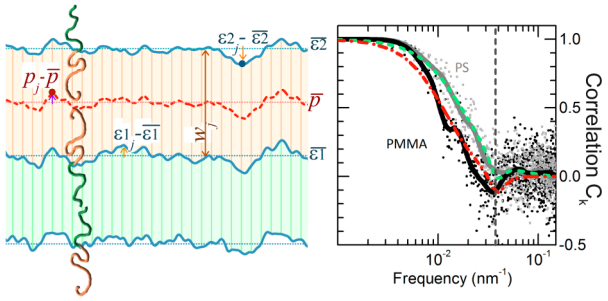

INTRODUCTION

Self-assembled patterns from block copolymers (BCPs) inevitably exhibit some type of roughness that originates from thermal fluctuations in the system. Such fluctuations are the focus of attention in academic and industrial research alike given the broad impact of this class of self-assembling materials. In the lithographic community, line roughness is a topic of technological relevance since directed self-assembly (DSA) of BCPs is being considered for the nanofabrication of magnetic recording[1] and semiconductor[2] devices where roughness specifications are stringent. For the soft-matter physics community, symmetric BCPs represent a playground to study thermal fluctuations at polymer interfaces in a system with a peculiar layering structure: BCPs stack similarly to smectic A materials, but the layering is associated more with the phase separated interfaces which reside in the middle of the molecules, rather than at the molecular ends. The layering of BCPs also resembles that of bilayer membranes[3] or polymersomes,[4] but with the end chains of one bilayer participating in the core membrane of the next bilayer. Despite its relevance, the behavior of line roughness in block copolymers has not been fully captured by a model that can predict and explain the various parameters that contribute to the thermal fluctuations that are perceived as roughness in the final pattern.

Because of the multidisciplinary interest in the topic, studies on line roughness of BCP films have been approached from various disciplines (e.g., lithography, polymer physics, and soft matter), each placing different levels of emphasis on either line edge, line width, or line placement roughness (LER, LWR, or LPR, respectively) but also with some efforts to bridge among the different fields. For instance, in the patterning and lithographic communities, emphasis tends to concentrate more heavily at measuring and characterizing LER and LWR. This approach comes as a natural extension from photoresist concepts.[5,6] Many reports in this field have been limited to metrology and characterization,[7−10] but contributions have been important in terms of describing the observed power spectral density (PSD) and the correlations between opposite edges of a single domain.[11,12] In the polymer physics community, various studies have been based on models describing fluctuations at polymer/polymer interfaces,[13,14] which relate to the LER of a single interface. Experimentally, Stein et al. reported on a study that incorporated contributions of capillary roughness to describe LER in BCP films.[15] Additional theoretical and computer simulation work has been done using models specific to the microphase separation of block copolymers in an attempt to describe the PSD of LER and LWR.[16−20] Among these, Bosse[17] proposed a phenomenological model that adds the PSD of interface-only capillary waves to the PSD of bulk fluctuations characteristic of BCPs, capturing some previously observed attributes such as a "resonant" frequency near the pitch frequency. Additional experimental, numerical, and theoretical work has also been pursued to establish a connection between the guiding patterns in DSA and the final structures.[20−26] However, emphasis has been largely placed on LER and LWR, and less attention has been paid to the significance of LPR. There have also been attempts to characterize the decay of the PSD with a power law

Received: November 4, 2016
Revised: January 6, 2017
Published: January 27, 2017

behavior with a single characteristic exponent[15,20,27] (as in the capillary wave example) that may neglect other contributions or sources of correlations. By contrast, the soft matter physics community has also made important contributions to the roughness topic through the study of thermal fluctuations in bilayer membranes.[28] An interesting aspect of the bilayer membranes is that it focuses on a definition of variables (undulatory and peristaltic normal modes) that puts LPR and LWR (not LER) as the fundamental expressions of the fluctuations in the system. Furthermore, the PSD of a bilayer membrane contains both capillary and membrane bending fluctuations that add texture to the PSD curve beyond a simple power law decay. Srinivas et al.[29] have pointed out that a bilayer membrane model can capture attributes of line roughness in BCP patterns.

In this article, our goal is to describe the thermal fluctuations of lamellae-forming BCP thin films, borrowing concepts from bilayer membranes, polymer physics, and lithography. We focus on undirected patterns (i.e., "fingerprint patterns") to show that the thermal fluctuations inherent to BCP films can be described with a model similar to those used for unconstrained bilayer membranes. The work here will help in understanding roughness fluctuations as originating from the BCP bilayers alone, without the influence of external fields. The case of directed self-assembly where the influence from the guiding pattern needs to be accounted for as an additional external field will be addressed in a future publication. We regard this study as a first step toward a comprehensive understanding of line roughness in block copolymer lithography. While the roughness of finished device elements will depend on a superposition of multiple factors such as pattern formation, selective block removal, and pattern transfer, the first source of roughness in BCP lithography stems from the intrinsic thermal fluctuations discussed here. The article is organized as follows: First, we start by reviewing the standard definitions for LER, LWR, and LPR in real and reciprocal space and the linear correlation coefficient as used in the lithography community.[1,6] We then point to an analogy for the linear correlation coefficient in reciprocal space that will be useful to capture correlations between adjacent domains as a function of frequency. Next, we propose a phenomenological model to describe LWR and LPR. We use the expression for the peristaltic modes of a bilayer membrane[28,30] to represent LWR, but recognizing that the bilayer is formed by a BCP melt subject to composition fluctuations, we followed Bosse's[17] example and added an expression for composition fluctuations to the peristaltic fluctuations to fully capture the LWR spectrum of BCPs. Lastly, we associate the undulatory modes of bilayer membranes[28,30] to the LPR spectrum, but we do it in a way that preserves the mathematical correlations between neighboring domains. We tested the model by fitting the PSDs of PS-*b*-PMMA thin films with three different pitch values. We find the model captures many of the important features observed in experimental data offering also a way to understand the contributions of some bulk and interfacial physical properties of the polymers to the perceived roughness.

EXPERIMENTAL SECTION

We studied the line roughness in thin films of symmetric poly(styrene-*b*-methyl methacrylate) (PS-*b*-PMMA) BCPs with three different pitch values (L_0 = 22, 25, and 27 nm).[31] PS-*b*-PMMA with L_0 = 22, and 25 nm and the OH-terminated random brush PS-*r*-PMMA-OH were received as solutions in propylene glycol methyl ester acetate (PGMEA) from EMD Performance Materials Corp. PS-*b*-PMMA with L_0 = 27 nm (M_n = 25-*b*-26 kg/mol and polydispersity index PDI = 1.06) was purchased from Polymer Source Inc. and was dissolved in toluene at 1.5 wt %. An ∼20 nm thick film of PS-*r*-PMMA-OH was spin-coated onto Si substrates and annealed for ∼30 min at 200 °C. The nongrafted excess of PS-*r*-PMMA-OH was rinsed with *N*-methyl-2-pyrrolidone (NMP) solvent in an ultrasonic bath. PS-*b*-PMMA thin films (one for each pitch value) were spin-coated to a thickness of ∼30 nm and annealed at 270 °C in a vacuum with a 10 mTorr nitrogen background pressure. The samples were taken out of the oven and quickly quenched by placing them on a metal block at room temperature. It is assumed that the observed morphology and roughness after quenching closely resemble the last state during annealing. Scanning electron microscopy (SEM) images were acquired on a ZEISS Ultra SEM operated at 1 kV (resolution ∼1.5 nm). The original image size was 3072 × 2304 pixels with a pixel size of 0.879 nm. Representative zoomed-in portions of the SEM micrographs for each L_0 value are shown in Figure 1.

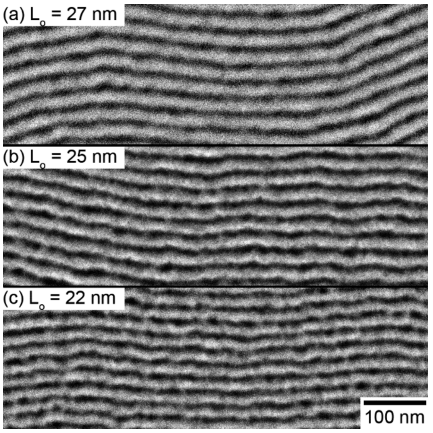

Figure 1. Top-down scanning electron micrographs of lamellar stripes from PS-*b*-PMMA block copolymers have a pitch of (a) 27, (b) 25, and (c) 22 nm. Light areas correspond to PS domains. The area shown here is only a small fraction of the analyzed area for each image.

Line roughness was measured from square SEM images 1.8 μm (2048 pixels) in lateral size cropped from the original files. For each sample, multiple (4−6) images were collected at random locations on the sample. The images were captured in areas where the lamellar pattern with mostly a single orientation would span the entire field of view. The stripes from the block copolymer lamellae were oriented generally perpendicular to the fast scan direction of the SEM (i.e., rotated ∼90° from their displayed orientation in Figure 1). The location of the PS/PMMA interface as captured by the SEM was extracted using a custom-made image processing routine in Mathematica described elsewhere.[32] During edge detection, a 2D Gaussian filter with a 2-pixel standard deviation was applied to minimize high-frequency aliasing. For the calculation of the PSDs, the line profiles were weighted by a Hann window to minimize spectral leakage[33] (the artifact in the PSD arising from truncating the data to a finite segment). All the detected edges in a single image were fitted to straight lines with the same slope to minimize detrending aliasing.[34] The power spectral density profiles of all lines in a single image were averaged to generate a single plot to minimize uncertainty[33] (each of these averages is shown with a unique symbol in the plots of this work). Because of the resolution of the images, noise, and filtering, aliasing was significant at frequencies above 0.2 nm^{-1}, so the frequency range from 0.2 to 0.56 nm^{-1} was discarded and it is not shown.

RESULTS AND DISCUSSION

Line Roughness Definitions in Real and Reciprocal Space. Line edge, width, and placement are defined according to the description in Figure 2 and following standard

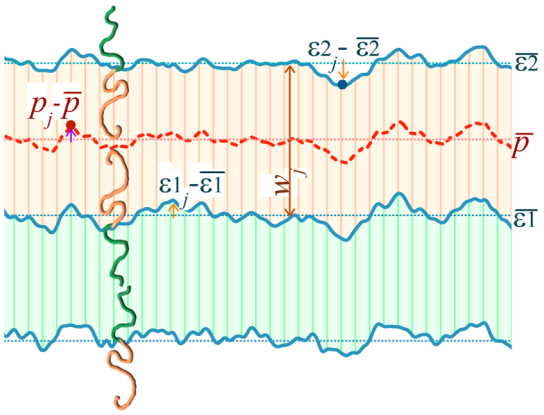

Figure 2. Cartoon representation of a bilayer membrane configuration in a lamellar block copolymer as well as edge, ε, width, w, and placement, p, definitions. The chain blocks in the center of one domain (orange ends) define one of the alternating lines (or membranes) in the striped pattern. The chain ends on the outer side would in turn participate of the formation of the adjacent line (green ends), thus forming a stack of adjacent membranes.

definitions.[1,6,35] Briefly, the line edge, ε, represents the interface between the PS and PMMA domains. At any point j, the width w_j and placement p_j are defined as

$$w_j = (\varepsilon 2_j - \varepsilon 1_j); \quad p_j = \frac{\varepsilon 1_j + \varepsilon 2_j}{2} \tag{1}$$

where $\varepsilon 1_j$ and $\varepsilon 2_j$ represent the sampled points of opposite edges (in a direction perpendicular to the best fit line of all sampled points) of either a PS or PMMA line (see Figure 2). In real space, the line edge, width, and placement roughness are related to the variance of the residuals:

$$\sigma_u^2 = \frac{1}{N-1}\sum_j (u_j - \bar{u})^2 \tag{2}$$

where u may stand for $\varepsilon 1$, $\varepsilon 2$, w, or p as appropriate and N represents the total number of sampled points. In lithography, it is common practice to define the line edge (or width) roughness as the 3σ value.[6] Following the above definitions, the three variances relate to each other:

$$\sigma_\varepsilon^2 = \frac{\sigma_w^2}{4} + \sigma_p^2; \quad \sigma_w^2 = 2\sigma_\varepsilon^2 - 2c\sigma_\varepsilon^2; \quad \sigma_p^2 = \frac{1}{2}\sigma_\varepsilon^2 + \frac{1}{2}c\sigma_\varepsilon^2 \tag{3}$$

where c is the linear correlation coefficient between the two edges[6] and where $\sigma_\varepsilon = \sigma_{\varepsilon 1} = \sigma_{\varepsilon 2}$ in the limit of large N for self-similar systems. We also note that in the patterns formed by a symmetric PS-*b*-PMMA BCP we will have two sets of variables: one to represent the width, placement, and correlation of the PS domains (s) and one for the PMMA domains (m), while the edges, of course, will be common to both domains (see Figure 2).

In frequency domain, the discrete power spectral density (PSD) is calculated as the squared magnitude of the Fourier transform of the feature residuals (edge, width, or placement):

$$G_u(f_k) = \frac{2\Delta}{N^2}|U_k|^2; \quad k = 1, 2 \ldots \frac{N}{2} - 1 \tag{4}$$

where, again, u may stand for ε, w, or p. U_k is the corresponding discrete Fourier coefficient of spatial frequency f_k, Δ is the sampling step, and U_k may represent E_k, W_k, or P_k for edge, width, or placement, respectively.

We also note that in reciprocal space the relationship between $G_\varepsilon(f_k)$, $G_p(f_k)$, and $G_w(f_k)$ parallels that of the variances in real space (eq 3). As demonstrated in the Supporting Information, we can write the following relationships in analogy to eq 3:

$$\begin{aligned} G_\varepsilon(f_k) &= \frac{G_w(f_k)}{4} + G_p(f_k) \\ G_w(f_k) &= 2G_\varepsilon(f_k) - 2C_k G_\varepsilon(f_k) \\ G_p(f_k) &= \frac{1}{2}G_\varepsilon(f_k) + \frac{1}{2}C_k G_\varepsilon(f_k) \end{aligned} \tag{5}$$

where C_k is a correlation coefficient in reciprocal space at frequency f_k. C_k can be written in terms of $G_p(f_k)$ and $G_w(f_k)$ or in terms of the edge Fourier coefficients $E1_k$ and $E2_k$ as follows (see Supporting Information for details):

$$C_k = \frac{4G_p(f_k) - G_w(f_k)}{4G_p(f_k) + G_w(f_k)} = \frac{E1_k E2_k^* + E1_k^* E2_k}{|E1_k|^2 + |E2_k|^2} \tag{6}$$

After some algebra shown in the Supporting Information, it can be shown that $C_k = \cos(\alpha_{1k} - \alpha_{2k})$ where $(\alpha_{1k} - \alpha_{2k})$ is the phase difference between the Fourier components of opposite edges at frequency f_k. C_k is a convenient form to visualize the correlations between opposite edges at each frequency. C_k ranges from 1 to -1, representing the range from fully correlated to fully anticorrelated edges, respectively.

Experimental Measurements. Figure 3 contains three columns displaying the PSDs and C_k plots for block copolymer samples having a pitch of L_0 = 27, 25, and 22 nm. In the first column (L_0 = 27), plot (a) displays the PSD curves for placement G_p and width G_w for the PS stripes, while plot (b) corresponds to the PMMA stripes. Plot (c) shows the edge PSD, G_ε. Plot (d) is the correlation coefficient in frequency domain, C_k for both the PS (gray) and PMMA (black) stripes. The second column shows the corresponding plots (e–h) for L_0 = 25 nm and the third column plots (i–l) correspond to L_0 = 22 nm. The data were collected from multiple (4–6) SEM images taken at different locations on each sample. The number of lines measured in each image varied depending on the ability to detect the PS/PMMA interfaces and the ability to locate large areas with no dislocations or disclinations. Each symbol in the PSD curves corresponds to the average PSD of all detected lines in one image. We note a few properties of the PSD plots: At low frequencies up to a characteristic frequency f_l ($\sim 10^{-2}$ nm^{-1}), the placement fluctuations diverge with a power law $\sim f^{-4}$, while the width saturates with constant amplitude as a consequence of the finite size of the polymer chains. Thus, at the lower frequencies ($f < f_l$) $G_p \gg G_w$ resulting in high correlation values (note that $C_k \approx 1$ when $G_p \gg G_w$ according to eq 6). At the mid-frequencies $f_l < f < f_h$ (where $f_h \sim 10^{-1}$ nm^{-1}) G_p bends, G_w decays, and C_k drops. C_k reaches a minimum at a frequency of the order of $1/L_0$, while above $1/L_0$, C_k tends to zero, indicating that the edges are becoming uncorrelated. As it will be explained later, it is this mid-frequency range the one that captures the characteristic modes of a bilayer membrane, and hence it will become the center of our attention for the rest of this work. For frequencies higher than $\sim 10^{-1}$ nm^{-1}, we cannot draw any conclusions since that part of the spectrum is affected by the filtering used during

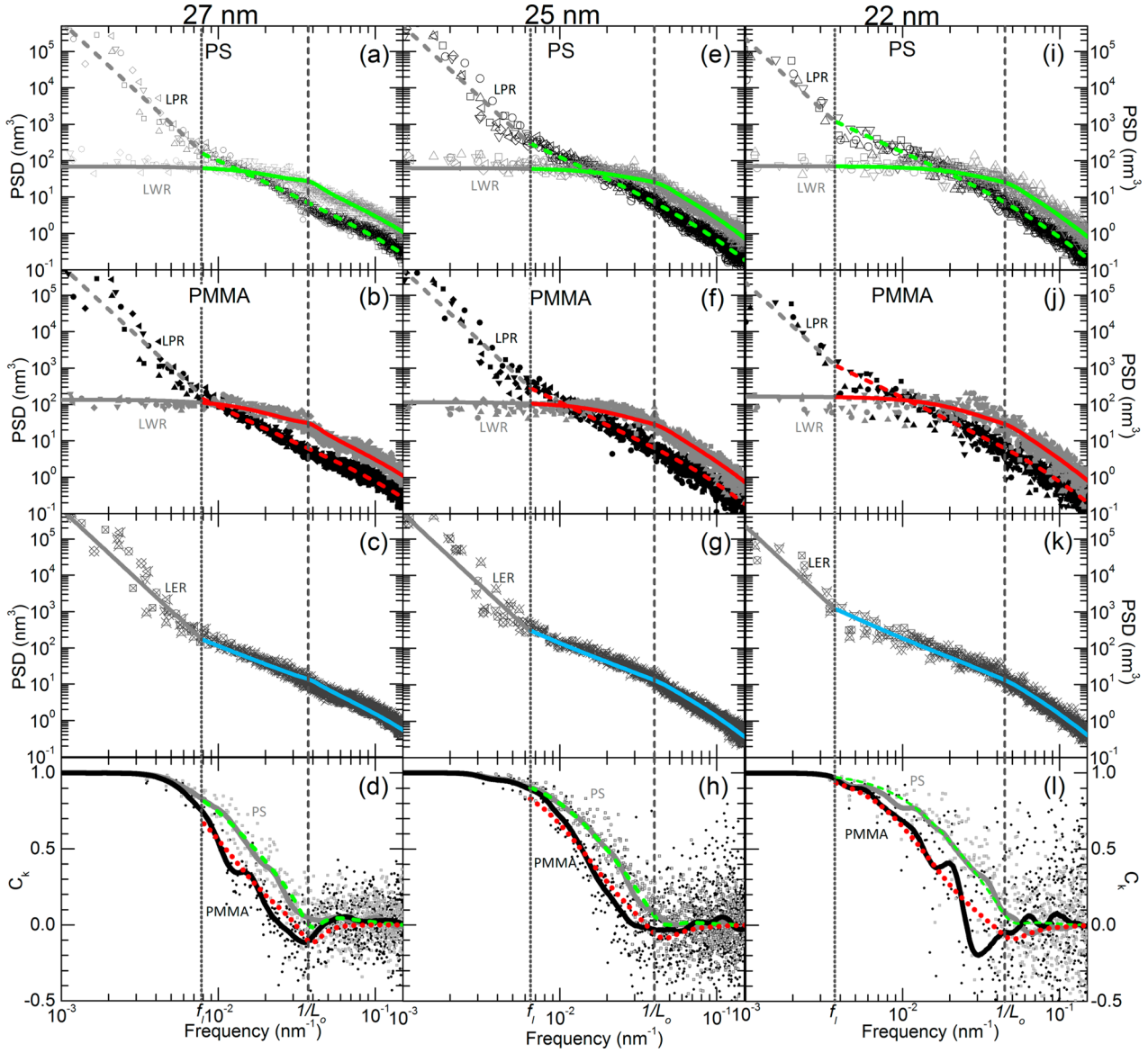

Figure 3. Line roughness of PS-*b*-PMMA films. The three columns correspond to the plots for the samples having a pitch, L_0, of 27 nm (a–d), 25 nm (e–h), and 22 nm (i–l). The first (top) plot in each column shows the placement (black) and width (gray) roughness PSD for the PS lines. The second plot in each column shows the corresponding placement and width roughness PSDs for the PMMA lines. The third plot is the edge roughness PSD. The bottom, fourth plot shows the correlation coefficient in reciprocal space, C_k, for PS (gray) and PMMA (black). The solid gray and black C_k curves are smooth averages of the data from all images. The dashed green and red dotted C_k curves are the best fit to the model in the frequency range $f_l > f > f_h$. The colored PSD curves in the first three plots of each column are the model curves using the parameters obtained from the best fit to C_k. The lower frequencies $f < f_l$ were not used for the fit. The transition to a f^{-4} power law in G_p for $f < f_l$ (gray, dashed line in G_p) was used only to pinpoint the persistence length ($f_l = 1/l_p$).

image processing and may also contain other sources of error from the image acquisition process;[33] hence, we restrict our plots up to f = 0.2 nm^{-1}. We would also like to further comment on the lower frequency portion of the spectra before we continue. Because the BCP patterns are unguided, the polymer stripes (bilayers) eventually diverge in a random walk-like behavior that is reflected on G_p (and G_ε) diverging as f^{-4} toward the low frequencies ($f < f_l$). Consequently, the PSD plots may suffer from leakage effects at the low frequency end of the spectrum.[33] We applied a Hann window to minimize this artifact, but we also point out that any leakage in the lower part of the spectrum is not expected to affect our studies significantly. First, we note that if our measurements had significant leakage, it would show not only on the G_p spectrum but also on G_w as a result of width measurements over unintended slanted or "diagonal" cuts across the width of the stripes. However, the G_w spectrum maintains a constant saturation value toward the lower frequencies without any significant deviation. Second, the relevant frequencies for the purpose of the bilayer membrane model at the core of this work are the mid-frequencies in the range $f_l < f < f_h$, where G_p no longer decays as f^{-4} and where C_k drops below 1. These mid-frequencies correspond to length scales for which the lines (or bilayer membranes) are considered generally flat, as it will be explained later, and thus are expected to have minimal leakage effects. Additionally, we repeated our measurements cropping the size of the image from ~1 to ~0.5 μm and observed no significant changes in the shape of the average PSD curves.

Model. Symmetric BCPs stack in ways similar to bilayer membranes which have characteristic thermal fluctuations. At the same time, BCPs constitute a microphase separated system that will also be subject to the characteristic thermal bulk composition fluctuations of phase segregating materials. One could thus expect line roughness in BCPs to be a consequence of both effects. Let us consider the fluctuations in the membrane-like structure first. The striped patterns formed by symmetric BCPs can be seen as the result of multiple, coupled membranes stacked one after the next. Thermal fluctuations in isolated lipid bilayers and polymersome membranes have been studied extensively.[3,36] In such membranes, it is common to distinguish between undulatory and peristaltic modes,[28]. The membrane can be fully described using two normal variables. The first normal variable, ${}^1/_2(\varepsilon 1_j + \varepsilon 2_j)$, describes the undulatory modes and corresponds to the placement variable as defined in eq 1. The second normal variable, ${}^1/_2(\varepsilon 2_j - \varepsilon 1_j)$, describes the peristaltic modes and corresponds to half the width as defined in eq 1. It is therefore tempting to associate the undulatory and peristaltic modes of a bilayer membrane to the LPR and LWR of block copolymer patterns, respectively. However, additional care needs to be taken to capture the correlations between consecutive edges and the relationships between consecutive lines (i.e., C_k and the relationships in eq 5). The lamellar structures of block copolymers can be regarded as a special case of stacked bilayers where the end chains of one bilayer contribute to the core of the next bilayer with opposite tone. The interactions and cross-talk that arise between the stacked bilayers are reflected in the correlations between consecutive edges with a characteristic correlation coefficient for one domain (i.e., C_k^s for PS) and a different one for the second domain (i.e., C_k^m for PMMA).

Previously, Bosse[17] suggested a phenomenological model to describe the LER in block copolymers. According to Bosse, interfacial modes (those arising from interfacial tension) were added to the bulk composition fluctuation modes. While this model shows some of the features present in the PSD of block copolymers, it does not identify the correlations between edges or the differences between domains or the width roughness of each domain. Furthermore, composition fluctuations affect the local volume of a given domain, and thus it may be more appropriate to add the composition fluctuations to the width roughness rather than to the edge roughness. Here, we propose to use the peristaltic modes of a bilayer membrane model to describe the width roughness adding the composition fluctuation modes to it. We also use the undulatory modes to describe the placement roughness. Once width and placement are described, edge roughness is mathematically determined from eq 5.

We begin with an expression for the PSD of the width roughness for the "x" domain where x should be replaced with an s to indicate a PS domain or an m to represent a PMMA domain:

$$G_w^x(f) = \frac{4k_BT/t}{\kappa_x(2\pi f)^4 + \gamma(2\pi f)^2 + \eta_x} + \frac{4A_x}{\xi^2\left(\frac{L_0}{2\pi}\right)^2\left[(2\pi f)^2 - \left(\frac{2\pi}{L_0}\right)^2\right]^2 + \left(1 - 2\xi^2\left(\frac{2\pi}{L_0}\right)^2\right)}; \quad f < f_h \tag{7}$$

The first term in eq 7 corresponds to the peristaltic modes of a bilayer membrane[29,30,37] with a peristaltic bending modulus κ_x, an interfacial tension γ, and a restoring field η_x. Note that to keep the variables in the conventional form used in lithography, we chose to use the spatial frequency $f = 1/\lambda$ as the independent variable instead of the conventional wavenumber $q = 2\pi/\lambda$. Additionally, the factor of 4 in the numerator arises from the factor of 2 difference in our definition of "width"; i.e., in the standard bilayer formalism,[28] the "width" is defined as $(\varepsilon_2 - \varepsilon_1)/2$ and not as defined in eq 1. Lastly, t corresponds to the film thickness which arises from the definition of the free energy of the membrane[30] following the fact that here we treat the membrane as a one-dimensional object (see Supporting Information for a demonstration). In the standard bilayer formalism, the membrane is treated as a two-dimensional object, but our SEM images show only the interface edges that reside at the top of the film forcing us to treat the membranes as one-dimensional objects, assuming that the second dimension along the thickness of the film is uniform (see Supporting Information). We note that by representing the striped patterns as one-dimensional bilayer membranes, we do not expect to be missing much more than just a constant factor: the PSD of thermal fluctuations in one and two dimensions share the same functional form and differ only by a factor of $1/t$ (see Supporting Information). As a consequence of the one-dimensional treatment, the units of G_w are in nm^3 instead of nm^4 as it is found in the membrane literature. It is also important to note that the peristaltic modes are valid up to a cutoff frequency f_h of the order of a molecular size at which point the fluctuations are dominated by uncorrelated molecular scale protrusions and are not described by this continuous model.[28,38,39] The C_k plots in Figure 3 indeed tend to zero at high frequencies.

The second term in eq 7 corresponds to the composition fluctuations as derived by Bosse[16] where ξ is a parameter associated with the interfacial width and A_x is a coupling constant that contains the thermal energy and the constant to couple the composition fluctuations to the width roughness. We arbitrarily kept a factor of 4 for symmetry with the first term. It is interesting to note that the functional form of both terms is the same, with a denominator containing a fourth power term, a quadratic term, and a constant term with the exception that in the composition fluctuations the quadratic coefficient is negative producing a "resonance" frequency at the pitch frequency.

For the PSD of the placement roughness, we first note that by virtue of eq 5:

$$G_\varepsilon = 1/4G_w^s + G_p^s = 1/4G_w^m + G_p^m$$
$$\Rightarrow G_p^s - G_p^m = 1/4(G_w^m - G_w^s) \tag{8}$$

which tells us that the placement PSDs "split" with a gap between $G_p^s$and G_p^m that is 1/4 of that between G_w^m and G_w^s, the extent of which is dictated by the correlation coefficients. A good model for line roughness in block copolymer films needs to be able to capture the relationships expressed in eq 8. Assuming that the combined placement PSDs G_p^s and G_p^m are a reflection of the undulations in the system, we define

$$G_{\text{und}}(f) = (G_p^s + G_p^m)/2 \tag{9}$$

Next we propose to use the undulatory modes of bilayer membranes[28,37,39] to fit G_{und}:

$$G_{\text{und}}(f) = \frac{k_B T/t}{\kappa_c (2\pi f)^4 + \gamma (2\pi f)^2}; \quad f_l < f < f_h \tag{10}$$

where κ_c is a bending modulus for the undulatory modes and the rest of the symbols have the same meaning as before. Note that in this case the expression for the undulatory modes has no restoring field, and thus the amplitude of the PSD diverges toward lower frequencies. Equation 10 is only valid between two cutoff frequencies: $f_l < f < f_h$, where $f_l = 1/l_p$, with l_p representing the persistence length and f_h as defined before. The persistence length is the region for which the membrane can be considered generally "flat" and where the Monge representation is valid.[30] For length scales larger than the persistence length, the membrane unwinds in patches of size l_p, the surface tension becomes irrelevant ($\gamma = 0$), and the intensity goes purely as[40] $\sim f^{-4}$ (i.e., the system can be seen as a random walk of membrane patches of size l_p). We observe this $\sim f^{-4}$ behavior in the low frequency portion of the LPR spectra (Figures 3), suggesting that the persistence length will be in the range of 100−300 nm for the three samples. We note that we are most interested in the fluctuations occurring in the frequency range $f_l < f < f_h$ which represent the oscillations of a bilayer membrane. It is in this range where the membrane can be considered generally flat and where we expect to apply our phenomenological model to gain insights into the physical properties that contribute to the thermal fluctuations. In our plots, we show the full range to lower frequencies only to show that indeed we observe the random walk behavior of the membrane patches.

From eqs 8 and 9 we obtain expressions for the placement PSDs of both the PS and PMMA domains:

$$G_p^s(f) = G_{\text{und}}(f) + \frac{1}{8}[G_w^m(f) - G_w^s(f)]$$
$$G_p^m(f) = G_{\text{und}}(f) - \frac{1}{8}[G_w^m(f) - G_w^s(f)] \tag{11}$$

Lastly, the expressions for the correlations in reciprocal space (or phase difference) follow from substituting eqs 7, 10, and 11 into eq 6 with C_k^s for the PS lines and C_k^m for the PMMA lines.

Fitting the Model to the Experimental Data. We fitted the proposed model to the roughness data as follows. For each set of samples with the same pitch L_0, the average $(G_p^s + G_p^m)/2$ was computed from the data. The mid-frequencies $f_l < f < f_h$ were fitted to eq 10 with fitting parameters γ and κ_c. In order to determine l_p, the low frequency portion of the curve $f < f_l$ was also fitted to eq 10 with $\gamma = 0$, and $f_l = 1/l_p$ was established as the value for which the two fits yielded a continuous curve. Note that the low frequency portion of the curve was only used to determine f_l. There is no other use or information we extract from the low frequency part of the G_p spectrum since the relevant information resides in the mid-frequencies at length scales below l_p.

The rest of the parameters (κ_s, κ_m, η_s, η_m, ξ, A_s, A_m) are obtained using the expressions for C_k^s and C_k^m. To simultaneously fit both expressions, the values for $C_k^s(f)$ were artificially mirrored to the negative frequencies, i.e., $C_k^s(f) = C_k^s(-f)$, and those for $C_k^m(f)$ were kept on the positive frequency. Then a single piecewise function was used for the fit:

$$C_k(f) = \begin{cases} C_k^s(-f); & -f_h < f < -f_l \\ C_k^m(f); & f_l < f < f_h \end{cases} \tag{12}$$

We further simplified the fit by reducing the number of fitting parameters with the following assumptions. If we set the frequency $f_h = 4/L_0$ (i.e., of the order of the block length) at which correlations vanish for both $C_k^s(f_h) = C_k^m(f_h) = 0$, then it can be shown that $A_s = A_m$ and

$$\kappa_x = \frac{1}{256\left(\frac{2\pi}{L_0}\right)^4} \left(\left(\frac{1}{256\kappa_c\left(\frac{2\pi}{L_0}\right)^4 + 16\gamma\left(\frac{2\pi}{L_0}\right)^2} - \frac{A_x t/(k_B T)}{\left(1 + 223\xi^2\left(\frac{2\pi}{L_0}\right)^2\right)} \right)^{-1} - 16\gamma\left(\frac{2}{L_0}\right)^2 - \eta_x \right)$$

reducing the number of fitting parameters to four: η_s, η_m, ξ, and A_s.

Once C_k is fitted, all parameters are known and each curve for the PSD can be reproduced from eqs 11, 10, and 7. The colored lines in Figure 3 correspond to the respective model equations using the best fitted parameters. Table 1 shows all of the relevant parameters. The first six parameters above the horizontal gap in Table 1 are the parameters obtained from the two fits (γ and κ_c from the fit to G_{und} and η_s, η_m, ξ, A_s from the fit to C_k), while κ_s and κ_m were determined from the condition $C_k^s(f_h) = C_k^m(f_h) = 0$ described above; $f_l = 1/l_p$ is the frequency at which G_{und} transitions to a f^{-4} power law as explained before. The exact values of L_0 as measured from the image analysis are also reported in Table 1 together with the thickness, t, of the spin-coated films.

Table 1. Model Parameters for Each Sample[a]

parameter	27 nm pitch	25 nm pitch	22 nm pitch
κ_c (J)	3.92×10^{-22} ($0.054\ k_B T$)	1.08×10^{-21} ($0.138\ k_B T$)	1.11×10^{-21} ($0.149\ k_B T$)
γ (J/nm^2)	6.73×10^{-22}	5.20×10^{-22}	3.85×10^{-22}
η_s (J/nm^4)	1.48×10^{-23}	1.66×10^{-23}	1.45×10^{-23}
η_m (J/nm^4)	7.47×10^{-24}	8.84×10^{-24}	6.16×10^{-24}
A_s (nm^3)	0.194	0.335	0.257
ξ (nm)	2.88	2.51	2.28
κ_s (J)	3.81×10^{-22}	1.11×10^{-21}	1.13×10^{-21}
κ_m (J)	3.90×10^{-22}	1.12×10^{-21}	1.14×10^{-21}
l_p (nm)	125	153.8	263.2
f_l (nm^{-1})	0.008	0.0065	0.0038
f_h (nm^{-1})	0.15	0.16	0.18
L_0 (nm)	26.8	25.0	22.3
t (nm)	30	30	30

[a]The parameters above the horizontal gap were obtained from the best fits to the model (κ_c and γ from eq 9 and η_s, η_m, ξ, A_s from eq 12).

In Table 2, we compare the rms roughness values for all three samples. In order for the rms values to be meaningful, they need to be computed from length scales smaller that l_p where the membranes are generally flat. We chose to scale the measurements with L_0 in order to provide a fair comparison among samples. We noted that $4L_0$ was always below l_p for all

Table 2. LWR, LPR, and LER rms Roughness Values and Linear Correlation Coefficients for PS-*b*-PMMA Samples with a Full Pitch of 27, 25, and 22 nm[a]

parameter	27 nm pitch	25 nm pitch	22 nm pitch
$3\sigma_w^s$ (nm)	4.3 ($0.16L_0$)	4.3 ($0.17L_0$)	4.6 ($0.21L_0$)
$3\sigma_w^m$ (nm)	5.0 ($0.19L_0$)	5.0 ($0.20L_0$)	5.7 ($0.26L_0$)
$3\sigma_p^s$ (nm)	3.9 ($0.14L_0$)	4.3 ($0.17L_0$)	5.0 ($0.22L_0$)
$3\sigma_p^m$ (nm)	3.7 ($0.14L_0$)	4.1 ($0.16L_0$)	4.7 ($0.21L_0$)
$3\sigma_e$ (nm)	4.4 ($0.17L_0$)	4.8 ($0.19L_0$)	5.5 ($0.25L_0$)
c_s	0.52	0.60	0.65
c_m	0.36	0.46	0.46

[a]The rms values are measured within the frequency range of $1/(4L_0) > F > 4/L_0$, so that all samples could be compared with each other.

samples. Thus, the rms values were computed in the frequency range $1/(4L_0) < f < f_h$ for each sample.

DISCUSSION

The model reproduces most of the features observed in the data with the dominant elements of the profile arising from the bilayer membrane behavior. We would like to focus the attention more on the functional form and on the relative values rather than on the absolute values of the fit in case model and data were still off by a constant. Nonetheless, we point out that the estimated values of the interfacial tension, γ, and the interfacial width, ξ, are within the expected order of magnitude. Extrapolating from previous studies on the temperature dependence of γ,[41,42] we expect the interfacial tension of PS/PMMA at 270 °C to be below 10^{-21} J/nm^2 (below 1 dyn/cm), which is indeed the case in all three samples (see Table 1). The interfacial width, ξ, is expected to be in the range of 3−5 nm from mean-field theory[43] and from experimental measurements.[15,44] Best-fit values to our model above give ξ values in the 2−3 nm range, which are not too far from the expected values. The bending moduli, κ_c, κ_s, and κ_m, on the other hand, while very close to each other, are rather low, about an order of magnitude below k_BT which may not be expected for bilayer membranes. It could be that at these high temperatures and due to the fact that the block copolymer is well above its glass transition temperature, the membrane is not stiff at all. The relatively low values of κ_c, κ_s, and κ_m mean that in the relevant frequency range of $f_l < f < f_h$, G_p and G_w will be mostly dominated by the interfacial energy term, γ, and/or the restoring field term, η_x, with κ_c and κ_x playing only a very minor role (see the denominator of eqs 7 and 10 and consider the case of low κ_c or low κ_x). Thus, there is a possibility that it may suffice to use an interfacial energy term only as proposed by Bosse,[17] with $\kappa_c = \kappa_s = \kappa_m = 0$, but then the slight bending of the PSD curve at higher frequencies would not be fully reproduced.

Because the width of the PS or PMMA domains at any given point cannot be larger than the length of the constituent molecules, the amplitude of the width fluctuations is not allowed to diverge beyond a length scale associated with the molecular size. This is the reason why the G_w^x spectra saturate toward the low frequencies as $f \to 0$. As the molecules coil or uncoil to accommodate for width fluctuations, there is a restoring field, η_x, arising from the entropic elasticity[45] of the molecules that will tend to restore the molecules to a more favorable coiling state. While the PS-*b*-PMMA chains used here are generally symmetric, the width of PMMA domains fluctuates more than that of PS as noted in the higher amplitude of G_w^m at lower frequencies and as seen in the rms $3\sigma_w$ values in Table 2. This is captured by the values obtained for the restoring field constants with $\eta_m < \eta_s$ (i.e., the PMMA domains appear softer than the PS ones). The different properties between the two blocks are beautifully captured in the C_k plots. At low frequencies, both curves are highly correlated. At frequencies of the order of f_l, the plots separate with C_k^m dropping faster, even reaching a negative value near $1/L_0$. This anticorrelated value is the result of the increased intensity in G_w^m arising from the composition fluctuations (second term in eq 7) at $f \sim 1/L_0$. It is also interesting to note that only the region around the resonant frequency from the composition fluctuations contributes significantly to G_w. At other frequencies, the contribution from the bilayer model (first term in eq 7) is much larger and dominates the spectrum. While the membrane model alone could capture most of the main features of the PSDs, inclusion of the composition fluctuations is necessary to reproduce the negative correlation values observed in C_k.

Another interesting feature of the C_k plots is the fact that the domain that exhibits the negative dip at $f \sim 1/L_0$ (PMMA) also maintains a lower correlation value throughout $f_l < f < f_h$ which may be a consequence of the mechanical properties of the polymer, e.g., $\eta_m < \eta_s$.

We also recognize that while the fit to C_k^s and C_k^m reproduces all of the main features of the data, it does not always capture the shoulder near f_l or the exact shape or position of the negative dip. This could be due to the fact that the C_k data are heavily scattered, and a proper smoothing would need many more samples to minimize the error in the PSDs,[33] or it could be that there is still something not captured by the model such as polydispersity effects[46] or the proximity to the order−disorder temperature for the smaller molecular weight polymers. Another open question about the model is the range of film thickness values for which it may be valid. Film thickness enters the free energy expression for the one-dimensional membrane (Supporting Information), implying that film thickness will impact the amplitude of the fluctuations, but in reality, our membranes are two-dimensional with fluctuations arising from all available modes. However, we show in the Supporting Information that the functional forms of the 1D and 2D problems are the same, differing only by a constant factor. Hopefully, this topic may motivate new modeling research in thermal fluctuations geared at describing the difference between both block domains and including the observed correlations and possibly the influence from the substrate.

We also compared the 3σ rms roughness values for all samples. In order to make a fair comparison between samples, we measured roughness values in the frequency range of $1/(4L_0) > f > f_h$ for all samples. We picked $4L_0$ as the cutoff length because we noticed $4L_0 < l_p$ for all samples. We found that the PMMA LWR is always higher than the PS LWR ($\sigma_w^m > \sigma_w^s$) which, as we discussed above, can be understood from the fact that $\eta_m < \eta_s$. We also found that the LWR stayed almost constant across samples with different pitch values. On the other hand, LPR values (and consequently LER) increased with decreasing pitch. Thus, LPR (and LER) were more sensitive to pitch changes than LWR. And in contrast to the LWR values, it is the PS LPR that is always higher than the PMMA LPR ($\sigma_p^s > \sigma_p^m$). This is a consequence of the G_p and G_w splitting discussed in eq 8, which in real space means that $(\sigma_p^s)^2 - (\sigma_p^m)^2 = 1/4[(\sigma_w^m)^2 - (\sigma_w^s)^2]$. The linear correlation coefficients are higher for the PS domains than for the PMMA domains for all

samples. This can be explained in part due to the relative "softness" of PMMA compared to PS ($\eta_m < \eta_s$). An interesting feature of the c values is that $\sigma_e^2 > \sigma_w^2$ when $c > 1/2$. In all samples, $c_s > 0.5$ while $c_m < 0.5$. So LER is always larger than LWR for the PS domains while the reverse is true for the PMMA domains. When $c > 3/5$, then $\sigma_p^2 > \sigma_w^2$; we only observe $c \geq 0.6$ for the PS domains in the 25 and 22 nm pitch samples.

Before concluding, a comment is pertinent regarding the contribution of the Flory−Huggins interaction parameter, χ, to the line roughness of block copolymers. In the equations used here, χ enters indirectly through two parameters: the interfacial tension, γ, and the interface width, ξ. According to mean-field theory,[43,47,48] $\gamma = (\chi/6)^{1/2} b\rho k_B T$ and $\xi = 2b(6\chi)^{-1/2}$, where b is the statistical length and ρ is the monomer density. While mean-field predictions and experimental measurements may still have many reported discrepancies,[49] the trend is a higher γ when χ is higher and a wider ξ when χ is lower. As we saw earlier, the undulatory modes G_{und} (eq 8) are mostly dominated by γ in the range $f_l < f < f_h$. Thus, a higher χ will indeed correspond to a lower amplitude in the undulatory modes. The placement roughness for each domain, G_p^x, could be lowered with a higher χ material since G_p^x comes mostly from the undulatory modes, G_{und}, plus a term coming from the difference between both G_w^x (eq 11). Note, however, that this is true here because the bending modulus, κ_c, is low; an alternative way to reach lower LPR is to increase κ_c (we do not know, however, if χ affects κ_c). Regarding the impact of χ on LWR, we observe that χ affects G_w through ξ and γ. The interfacial width, ξ, appears in the composition fluctuations (second term) in eq 7. When χ is lower, ξ is higher, resulting in a higher intensity of the resonant peak at $\sim 1/L_0$ as had been reported before,[18] although this effect of ξ on the width roughness occurs only over a very narrow range of frequencies. On the other hand, the peristaltic modes (first term in eq 7) dominates most of the G_w spectrum. In the peristaltic modes, γ (which contains χ) affects the decay of G_w mostly for frequencies above the pitch frequency ($f > 1/L_0$), while the restoring field, η_x, contributes the most to G_w given that it determines the saturation value of G_w at lower frequencies. Thus, the restoring field η_x dominates the contribution to the rms σ_w. While η_x should be related to the restoring force that brings the domain width back to its equilibrium value when the polymer chains try to uncoil or collapse, it is not clear how much χ contributes to this value. One could speculate that if there is any contribution from χ to η_x, it could be more significant only for small N values where the stretching at the interface becomes an important fraction of the entire domain width and an important fraction of the chain end-to-end distance. For large N, the coiling in the interior of the domain may screen what happens at the interface, making χ potentially less relevant. In short, χ would be only one of the elements influencing the intensity of the PSDs, but just how important χ is may also depend on the differences between the mechanical properties of the polymers, the frequency range considered for the PSD, and whether LWR or LPR is more important for the given application. Additional considerations may also arise once the assembly is directed by some guiding pattern that will confine the membranes to arbitrarily long, straight stripes. The membranes will attempt to unwind beyond l_p, but there will be an additional restoring force in G_p that will add pressure to the domains.[30,50] Finally, the roughness (LPR, LWR, and LER) observed in block copolymer films after self-assembly will not be the same as observed after one domain has been removed to generate a lithographic mask. We have seen that χ makes its most relevant contribution to roughness through the interfacial term γf^2 in the denominator of the undulatory and peristaltic modes. However, upon selective removal of one block, the interface is reconstructed to become the new surface of the remaining block. How much of the original capillary (interfacial) modes in the PSD remains after selective block removal will probably depend on the physical and chemical events characteristic of the method chosen to remove the one block.

CONCLUSIONS

In summary, we described the observed roughness in block copolymer thin films in light of a phenomenological model that includes the thermal fluctuations of a bilayer membrane and the thermal composition fluctuations of phase separated block copolymers. The width roughness is associated with the peristaltic modes described for bilayer membranes plus a term including composition fluctuations. The placement roughness follows the undulatory modes of a bilayer membrane with the particular PSD for PS and PMMA splitting by an amount that is proportional to the difference in G_w. The edge roughness then follows from the mathematical relationship in eq 5. The correlation coefficient in reciprocal space provides a spectrum that captures the relationship between placement and width roughness as well as the differences between the alternating domains, some of which reflect physical properties of the constituent polymers. While this phenomenological model may represent only an initial step, we hope that it motivates additional experimental and theoretical work toward a more rigorous and comprehensive understanding of line roughness and thermal fluctuations in block copolymer films.

ASSOCIATED CONTENT

Supporting Information

The Supporting Information is available free of charge on the ACS Publications website at DOI: 10.1021/acs.macromol.6b02399.

Demonstration of the parallel relationships in real and reciprocal space of the two sets of equations in eqs 3 and 5, including also a derivation of C_k; the PSDs of thermal fluctuations for 1D and 2D membranes differ only by a constant given by $1/t$ (PDF)

AUTHOR INFORMATION

Corresponding Author

*E-mail ricardo.ruiz@hgst.com (R.R.).

ORCID

Ricardo Ruiz: 0000-0002-1698-4281

Present Address

T.R.A.: Molecular Vista, Inc., San Jose, CA 95119.

Notes

The authors declare no competing financial interest.

ACKNOWLEDGMENTS

The authors thank B. Marchon, H. Gao, G. Doerk (HGST), and H. Yoshida (Hitachi Ltd.) for insightful discussions on roughness of BCPs. We also thank J. Yin, J. Kim, Y. Cao, and G. Lin from EMD Performance Materials Corp. for providing the random brush and the 25 and 22 nm pitch block copolymers.

REFERENCES

(1) Albrecht, T. R.; Arora, H.; Ayanoor-Vitikkate, V.; Beaujour, J.; Bedau, D.; Berman, D.; Bogdanov, A. L.; Chapuis, Y.; Cushen, J.; Dobisz, E. E.; Doerk, G.; Gao, H.; Grobis, M.; Gurney, B.; Hanson, W.; Hellwig, O.; Hirano, T.; Jubert, P.; Kercher, D.; Lille, J.; Liu, Z.; Mate, C. M.; Obukhov, Y.; Patel, K. C.; Rubin, K.; Ruiz, R.; Schabes, M.; Wan, L.; Weller, D.; Wu, T.; Yang, E. Bit-Patterned Magnetic Recording: Theory, Media Fabrication, and Recording Performance. *IEEE Trans. Magn.* **2015**, *51*, 1−42.

(2) Bencher, C.; Smith, J.; Miao, L.; Cai, C.; Chen, Y.; Cheng, J. Y.; Sanders, D. P.; Tjio, M.; Truong, H. D.; Holmes, S.; Hinsberg, W. D. Self-Assembly Patterning for Sub-15nm Half-Pitch: A Transition from Lab to Fab. *Proc. SPIE* **2011**, *7970*, 79700F.

(3) Daillant, J.; Bellet-Amalric, E.; Braslau, A.; Charitat, T.; Fragneto, G.; Graner, F.; Mora, S.; Rieutord, F.; Stidder, B. Structure and Fluctuations of a Single Floating Lipid Bilayer. *Proc. Natl. Acad. Sci. U. S. A.* **2005**, *102*, 11639−11644.

(4) Discher, B. M.; Won, Y.-Y.; Ege, D. S.; Lee, J. C.; Bates, F. S.; Discher, D. E.; Hammer, D. A. Polymersomes: Tough Vesicles Made from Diblock Copolymers. *Science* **1999**, *284*, 1143−1146.

(5) Mack, C. A. *Field Guide to Optical Lithography*; SPIE Press: Bellingham, WA, 2006; Vol. *6*.

(6) Bunday, B. D.; Bishop, M.; McCormack, D. W., Jr.; Villarrubia, J. S.; Vladar, A. E.; Dixson, R.; Vorburger, T. V.; Orji, N. G.; Allgair, J. A. Determination of Optimal Parameters for Cd-Sem Measurement of Line-Edge Roughness. *Proc. SPIE* **2004**, 5375.

(7) Tsai, H. Y.; Miyazoe, H.; Engelmann, S.; To, B.; Sikorski, E.; Bucchignano, J.; Klaus, D.; Liu, C. C.; Cheng, J.; Sanders, D.; Fuller, N.; Guillorn, M. Sub-30nm Pitch Line-Space Patterning of Semiconductor and Dielectric Materials Using Directed Self-Assembly. *J. Vac. Sci. Technol., B: Nanotechnol. Microelectron.: Mater., Process., Meas., Phenom.* **2012**, *30*, 06F205.

(8) Tsai, H.; Miyazoe, H.; Vora, A.; Magbitang, T.; Arellano, N.; Liu, C.-C.; Maher, M. J.; Durand, W. J.; Dawes, S. J.; Bucchignano, J. J. In *High Chi Block Copolymer Dsa to Improve Pattern Quality for Finfet Device Fabrication*; SPIE Advanced Lithography, International Society for Optics and Photonics: 2016; pp 977910−977910-7.

(9) Sunday, D. F.; Hammond, M. R.; Wang, C.; Wu, W.-l.; Kline, R. J.; Stein, G. E. Three-Dimensional X-Ray Metrology for Block Copolymer Lithography Line-Space Patterns. *J. Micro/Nanolithogr., MEMS, MOEMS* **2013**, *12*, 031103−031103.

(10) Xiong, S.; Chapuis, Y.-A.; Wan, L.; Gao, H.; Li, X.; Ruiz, R.; Nealey, P. F. Directed Self-Assembly of High-Chi Block Copolymer for Nano Fabrication of Bit Patterned Media Via Solvent Annealing. *Nanotechnology* **2016**, *27*, 415601.

(11) Peters, A. J.; Lawson, R. A.; Nation, B. D.; Ludovice, P. J.; Henderson, C. L. Simulation Study of the Effect of Molar Mass Dispersity on Domain Interfacial Roughness in Lamellae Forming Block Copolymers for Directed Self-Assembly. *Nanotechnology* **2015**, *26*, 385301.

(12) Constantoudis, V.; Kuppuswamy, V.-K. M.; Gogolides, E.; Pret, A. V.; Pathangi, H.; Gronheid, R. In *Challenges in Ler/Cdu Metrology in Dsa: Placement Error and Cross-Line Correlations*; SPIE Advanced Lithography, International Society for Optics and Photonics: 2016; pp 97781X−97781X-11.

(13) Semenov, A. N. Scattering of Statistical Structure of Polymer/Polymer Interfaces. *Macromolecules* **1994**, *27*, 2732−2735.

(14) Stamm, M.; Schubert, D. W. Interfaces between Incompatible Polymers. *Annu. Rev. Mater. Sci.* **1995**, *25*, 325−356.

(15) Stein, G. E.; Liddle, J. A.; Aquila, A. L.; Gullikson, E. M. Measuring the Structure of Epitaxially Assembled Block Copolymer Domains with Soft X-Ray Diffraction. *Macromolecules* **2010**, *43*, 433−441.

(16) Bosse, A. W. Thermal Composition Fluctuations in an Ordered Lamellar Mesophase. *Phys. Rev. E* **2012**, *85*, 042801.

(17) Bosse, A. W. Modeling the Power Spectrum of Thermal Line Edge Roughness in a Lamellar Diblock Copolymer Mesophase. *J. Vac. Sci. Technol., B: Nanotechnol. Microelectron.: Mater., Process., Meas., Phenom.* **2011**, *29*, 06F202.

(18) Bosse, A. W. Effects of Segregation Strength and an External Field on the Thermal Line Edge and Line Width Roughness Spectra of a Diblock Copolymer Resist. *J. Vac. Sci. Technol., B: Nanotechnol. Microelectron.: Mater., Process., Meas., Phenom.* **2011**, *29*, 031803.

(19) Patrone, P. N.; Gallatin, G. M. Modeling Line Edge Roughness in Templated, Lamellar Block Copolymer Systems. *Macromolecules* **2012**, *45*, 9507−9516.

(20) Patrone, P. N.; Gallatin, G. M. Response of Block Copolymer Thin-Film Morphology to Line-Width Roughness on a Chemo-epitaxial Template. *Macromolecules* **2014**, *47*, 4824−4829.

(21) Peters, A. J.; Lawson, R. A.; Ludovice, P. J.; Henderson, C. L. Detailed Molecular Dynamics Studies of Block Copolymer Directed Self-Assembly: Effect of Guiding Layer Properties. *J. Vac. Sci. Technol., B: Nanotechnol. Microelectron.: Mater., Process., Meas., Phenom.* **2013**, *31*, 06F302.

(22) Stoykovich, M. P.; Daoulas, K. C.; Muller, M.; Kang, H. M.; de Pablo, J. J.; Nealey, P. F. Remediation of Line Edge Roughness in Chemical Nanopatterns by the Directed Assembly of Overlying Block Copolymer Films. *Macromolecules* **2010**, *43*, 2334−2342.

(23) Daoulas, K. C.; Mueller, M.; Stoykovich, M. P.; Kang, H.; de Pablo, J. J.; Nealey, P. F. Directed Copolymer Assembly on Chemical Substrate Patterns: A Phenomenological and Single-Chain-in-Mean-Field Simulations Study of the Influence of Roughness in the Substrate Pattern. *Langmuir* **2008**, *24*, 1284−1295.

(24) Sunday, D. F.; Ashley, E.; Wan, L.; Patel, K. C.; Ruiz, R.; Kline, R. J. Template-Polymer Commensurability and Directed Self-Assembly Block Copolymer Lithography. *J. Polym. Sci., Part B: Polym. Phys.* **2015**, *53*, 595−603.

(25) Kato, T.; Sugiyama, A.; Ueda, K.; Yoshida, H.; Miyazaki, S.; Tsutsumi, T.; Kim, J.; Cao, Y.; Lin, G. In *Advanced CD-SEM Metrology for Pattern Roughness and Local Placement of Lamellar DSA*; SPIE Advanced Lithography, International Society for Optics and Photonics: 2014; pp 90501T−90501T-11.

(26) Doerk, G. S.; Liu, C.-C.; Cheng, J. Y.; Rettner, C. T.; Pitera, J. W.; Krupp, L. E.; Topuria, T.; Arellano, N.; Sanders, D. P. Pattern Placement Accuracy in Block Copolymer Directed Self-Assembly Based on Chemical Epitaxy. *ACS Nano* **2013**, *7*, 276−285.

(27) Bosse, A. W. Phase-Field Simulation of Long-Wavelength Line Edge Roughness in Diblock Copolymer Resists. *Macromol. Theory Simul.* **2010**, *19*, 399−406.

(28) Lindahl, E.; Edholm, O. Mesoscopic Undulations and Thickness Fluctuations in Lipid Bilayers from Molecular Dynamics Simulations. *Biophys. J.* **2000**, *79*, 426−433.

(29) Srinivas, G.; Swope, W. C.; Pitera, J. W. Interfacial Fluctuations of Block Copolymers: A Coarse-Grain Molecular Dynamics Simulation Study. *J. Phys. Chem. B* **2007**, *111*, 13734−13742.

(30) Safran, S. A. *Statistical Thermodynamics of Surfaces, Interfaces, and Membranes*; Addison-Wesley Pub.: 1994.

(31) Wan, L.; Ruiz, R.; Gao, H.; Patel, K. C.; Albrecht, T. R.; Yin, J.; Kim, J.; Cao, Y.; Lin, G. The Limits of Lamellae-Forming Ps-B-Pmma Block Copolymers for Lithography. *ACS Nano* **2015**, *9*, 7506.

(32) Ruiz, R.; Wan, L.; Lille, J.; Patel, K. C.; Dobisz, E.; Johnston, D. E.; Kisslinger, K.; Black, C. T. Image Quality and Pattern Transfer in Directed Self Assembly with Block-Selective Atomic Layer Deposition. *J. Vac. Sci. Technol., B: Nanotechnol. Microelectron.: Mater., Process., Meas., Phenom.* **2012**, *30*, 06F202.

(33) Mack, C. A. Systematic Errors in the Measurement of Power Spectral Density. *J. Micro/Nanolithogr., MEMS, MOEMS* **2013**, *12*, 033016−033016.

(34) Mack, C. A. More Systematic Errors in the Measurement of Power Spectral Density. *J. Micro/Nanolithogr., MEMS, MOEMS* **2015**, *14*, 033502−033502.

(35) Doerk, G. S.; Gao, H.; Wan, L.; Lille, J.; Patel, K. C.; Chapuis, Y. A.; Ruiz, R.; Albrecht, T. R. Transfer of Self-Aligned Spacer Patterns for Single-Digit Nanofabrication. *Nanotechnology* **2015**, *26*, 085304.

(36) Jain, S.; Bates, F. S. On the Origins of Morphological Complexity in Block Copolymer Surfactants. *Science* **2003**, *300*, 460−464.

(37) Marrink, S. J.; Mark, A. E. Effect of Undulations on Surface Tension in Simulated Bilayers. *J. Phys. Chem. B* **2001**, *105*, 6122−6127.
(38) Goetz, R.; Gompper, G.; Lipowsky, R. Mobility and Elasticity of Self-Assembled Membranes. *Phys. Rev. Lett.* **1999**, *82*, 221−224.
(39) Brochard, F.; De Gennes, P.; Pfeuty, P. Surface Tension and Deformations of Membrane Structures: Relation to Two-Dimensional Phase Transitions. *J. Phys. (Paris)* **1976**, *37*, 1099−1104.
(40) Gido, S. P.; Thomas, E. L. Lamellar Diblock Copolymer Grain-Boundary Morphology 0.2. Scherk Twist Boundary Energy Calculations. *Macromolecules* **1994**, *27*, 849−861.
(41) Carriere, J. C.; Biresaw, G.; Sammler, L. R. Temperature Dependence of the Interfacial Tension of Ps/Pmma, Ps/Pe, and Pmma/Pe Blends. *Rheol. Acta* **2000**, *39*, 476−482.
(42) Helfand, E.; Sapse, A. M. Theory of Unsymmetric Polymer–Polymer Interfaces. *J. Chem. Phys.* **1975**, *62*, 1327−1331.
(43) Semenov, A. N. Theory of Block Copolymer Interfaces in the Strong Segregation Limit. *Macromolecules* **1993**, *26*, 6617−6621.
(44) Sunday, D. F.; Kline, R. J. Reducing Block Copolymer Interfacial Widths through Polymer Additives. *Macromolecules* **2015**, *48*, 679−686.
(45) Ortiz, C.; Hadziioannou, G. Entropic Elasticity of Single Polymer Chains of Poly (Methacrylic Acid) Measured by Atomic Force Microscopy. *Macromolecules* **1999**, *32*, 780−787.
(46) The membrane model is a continuous model and does not describe polydispersity effects. Experimentally, without a systematic set of materials with various PDI values, we do not have a way to discern which parts of the spectrum are likely to be affected by polydispersity.
(47) Helfand, E.; Tagami, Y. Theory of the Interface between Immiscible Polymers. Ii. *J. Chem. Phys.* **1972**, *56*, 3592−3601.
(48) Helfand, E.; Tagami, Y. Theory of the Interface between Immiscible Polymers. *J. Polym. Sci., Part B: Polym. Lett.* **1971**, *9*, 741−746.
(49) Anastasiadis, S. H.; Gancarz, I.; Koberstein, J. T. Interfacial Tension of Immiscible Polymer Blends: Temperature and Molecular Weight Dependence. *Macromolecules* **1988**, *21*, 2980−2987.
(50) De Gennes, P. G.; Taupin, C. Microemulsions and the Flexibility of Oil/Water Interfaces. *J. Phys. Chem.* **1982**, *86*, 2294−2304.